Supporting Information for

Large-Area and Transferred High-Quality Three-Dimensional Topological Insulator $Bi_{2-x}Sb_xTe_{3-y}Se_y$ Ultrathin Film by Catalyst-Free Physical Vapor Deposition

Ngoc Han Tu[†], Yoichi Tanabe[†], Yosuke Satake[†], Khuong Kim Huynh[‡], Phuoc Huu Le[†], Stephane Yu Matsushita[†] and Katsumi Tanigaki[†, ‡**]*

†Department of Physics, Graduate School of Science, Tohoku University, Sendai, 980-8578, Japan.
‡WPI Advanced Institute for Materials Research, Tohoku University, Sendai 980-8577, Japan.

E-mail: ytanabe@m.tohoku.ac.jp, tanigaki@m.tohoku.ac.jp

TEL : +81-22-217-6173,

1. Materials and Methods

BSTS thin films were epitaxially grown on Fluorophlogopite mica ($KMg_3(AlSi_3O_{10})F_2$) by catalyst-free physical vapor deposition using dual tubes in a three–zone furnace under pressure of c.a. 0.1Pa. $Bi_{1.5}Sb_{0.5}Te_{1.7}Se_{1.3}$ single crystal grown by a slow cooling down method was employed as a source material. First, the 3g mixture of high – purity starting materials Bi (5N), Sb (5N), Te (5N), Se (5N) (Koujundo Chemical Laboratory CO., LTD) were sealed in an 5 cm - evacuated quartz tube with pressure ~ 10^{-2}Pa. Then the mixture was heated up to 850^0C and kept in 48 hours. During this 48 hours, the tube was shaken and rotated many times before quenching to room temperature. This procedure was repeated 6 times to obtain the homogeneous polycrystalline BSTS. Finally, the tube was again heated up to 850^0C for 24 hours and slowly cooling down to 550^0C with a cooling rate of 3^0C / h. Before completely cooling down to room temperature, it was annealed at 550^0C for 7 days to further improve the crystallinity. BSTS single crystal was characterized by the electrical transport measurements, energy dispersive X–ray (EDX) spectroscopy, X–Ray diffraction (XRD). Temperature dependence of electrical resistivity showed ~ 40 Ωcm higher than the previous report[1], representing the high bulk insulating states in the present bulk single crystal (**Fig. S1(a)**). For EDX measurements, EDX analyses revealed that BSTS films with the uniform chemical composition of Bi:Sb:Te:Se of 1.5:0.5:1.7:1.3 in atomic ratio were grown within the resolution of EDX (**Fig. S1 (b)**) . Clear (00ℓ) (ℓ=3n, where n in integer) diffraction peaks of BSTS (**Fig. S1(c)**) were observed. The Raman spectra showed the five peaks at 109, 125, 136, 156, 163 cm^{-1} shown in **Fig. S1(d)**, being consistent with the previous results [2].

As-grown BSTS films were exfoliated from mica substrates in a deionized water. For the thicker film ($t > 15$ nm), as-grown BSTS thin films were precedently dipped into a 2.38 % tetra-methyl ammonium hydroxide (NMD–W 2.38%) aqueous solution in several seconds until the outer edge of BSTS film began to be peeled off from the substrate. Morphology of BSTS films was observed by optical microscopy (Olympus BX51), scanning electron microscopy (JEOL JSM-7800F) and atomic force microscopy (AFM, SII NanoTechnology). Thickness of BSTS thin films was measured by a surface texture measuring instrument (Surfcom 1400G – Accretech) and AFM. The crystal structure and the composition of BSTS films were characterized by Raman spectroscopy (Labram HR-800, Horiba, 628 nm Laser excitation), X-Ray diffraction (Rigaku, SmartLab) and energy dispersive X–ray spectroscopy (JEOL JEM-2010 and JSM-7800F). Electrical transport measurements were performed by a

standard four probe method using a semiconducting devise analyzer (Agilent B1500), a nano-voltmeter (Agilent 34420A), and a signal generator (Keithley 6221) under magnetic fields below 9 T in the temperature range of 2 to 300 K. Six Au/ Cr (50/5 nm) electrodes were made by a thermal evaporation method using a metal mask.

2. Influence of an inner tube diameter d on the nucleation process

To clarify the effect of an inner tube on the nucleation process, we changed a size of an inner small tube with a diameter d from 0.4 cm to 1.5 cm while fixed amount of source materials (~ 15 mg) as well as other growth parameters. **Fig. S2** showed the results after 5 min growth with different inner tube diameters d. (Also see Fig. 2 in the main text) Island – like structures with small grain sizes (less than 1μm in the lateral size) and a large variation of thickness indicated by different contrast color were observed in the case of d = 0.4 cm. With an increase in d from 0.4 to 1 cm, two – dimensional nanoplates (NPs) with a lateral size ~ 2μm arranged in almost same orientation were obtained. The same contrast color from an optical photo image indicated that NPs have the almost same thickness. For d = 1.5 cm, an ultrathin and continuous film composed of well aligned NPs with ~ 3 nm thickness, was obtained. The reason for such a growth mode transition from the three – dimensional island mode to the two dimensional layer – by layer mode is attributed to the change of the density of BSTS gas attaching on the surface of a mica substrate, depending on an inner tube diameter d. By fixing amount of source material and other growth parameter such as pressure, growth temperature, growth time, an amount of source material and pressure, d of the inner tube could be a control parameter to tune the density of BSTS vapor attaching on the surface of mica substrate. A smaller inner tube diameter would give a higher density of BSTS vapor on the growth substrate, resulting in the high nucleation and growth rate. Therefore, in the case of d = 0.4 cm, the a larger amount of BSTS vapor was attached on the mica substrate, leading to the high nucleation density with the large variation of the thickness as shown in **Fig. S2 (a)**. To reduce the nucleation rate, we enlarged the inner tube diameter to suppress amount of BSTS vapor attached on the mica substrate. As results, an uniform and a large area growth in the lateral dimention on the mica substrate was realized with an increase in the inner tube diameter.

3. XPS studies on $Bi_{2-x}Sb_xTe_{3-y}Se_y$ thin film

In order to clarify the surface oxidization effect in the present thin film growth and the film transfer process, X-ray photo emission spectroscopy (UL-VAC-PHI Inc. PHI5600, Al(Kα) source) was measured using BSTS thin film before and after the film transfer process.(**Fig. S5**) After the thin film growth, the as grown BSTS thin film ($1cm^2$) on the mica substrate was cutted in 4 mm^2 in the air for the film transfer process. After the film transfer process, both the as-grown film and the transferred film on the SiO_2/Si substrate were kept in the air for a half day to clarify the additional oxidization originating from the film transfer process. XPS measurements were performed with the 45° angle between the a sample and a detecter. The incident beem was focused to a spot about 5 - 6 mm^2 region. Clear O1s peak after the film transfer is originated from the background SiO_2/Si substrate. For the as-grown BSTS thin film, both the TeO_2 and Sb_2O_3 peak were detected for Te 3d and Sb 3d. After the film transfer process, no increase in the peak area for TeO_2 and Sb_2O_3 compared to those of the Te 3d and Sb 3d, indicating that the present film transfer method does not give further oxidization. A typical electron escape depth of 1.8 nm for Al(Kα) source[3] as well as the 45° angle between a sample and a detecter suggest that the surface of BSTS thin film (~ 1QL ~ 1nm) tends to be oxidized. This natural oxidization is due to the sample aging in the air, being consistent with the previous report in Bi_2Se_3 nano ribbon[3].

4. Thickness variation of the electronic states for the BSTS ultrathin film

In order to clarify electronic states of BSTS ultrathin film, we measured the temperature dependence of the electrical resistance for the various thickness samples. (**Fig. S7**) For the 30 nm thick BSTS, the semiconducting-like R_{xx} -T curve is observed at high temperature, indicating a significant contribution of the insulating bulk electronic states. At low temperature, metallic-like behavior emerges. This is consistent with the increase in the carrier mobility for the metallic topological surface states. When the thickness was down to 10 -20 nm, the high temperature semiconducting-like behavior was suppressed and metallic behavior becomes dominant up to 300 K. This is due to a decrease in the contribution of the bulk states, resulting in the dominant contribution of the metallic topological surface states in the total conductance. Thus the metallic topological surface states takes place under the insulating electric back ground in the present BSTS ultrathin film[4]. When the thickness was

reduced below 3-4 nm, the R_{xx} - T curve shows the semiconducting-like behavior again. It is well known that the hybridization of the top and bottom surface is expected to open the energy gap on the topological surface states when the thickness reduced below the critical thickness[5]. In fact as shown in **Fig. 4 (c)** in the main text, V_G dependence of the R_{xx} for the 3 nm thick film showed ~ 10^4 high on/off switching ratio at 2 K. Since the R_{xx} at $V_G = 0$ V is comparable with the those of $Bi_{2-x}Sb_xTe_3$ ultrathin film (2 – 3 nm thick) where the hybridization gap was opened for the topological surface states[6], this high on/off switching ratio could be one of evidence for the massive Dirac fermion in the present BSTS ultrathin film. Because ~10^4 on/off switching ratio is record high in the 3D-TI materials and it is merit for the future application for the switching device.

5. Electric field effect induced Fermi level shift for the topological surface states

To examine the electric field effect induced Fermi level shift for the topological surface states, we measured the magnetoresistance for 18 nm thick film at various V_G. The magnetoresistance showed the weak antilocalization-like curvatures with the several quantum oscillations for $V_G = 0$, -120 and -150 V. (**Fig. S8**). After the subtracting the background magnetoresistance, the oscillatory part of the SdH oscillations were shown in **Fig. S9(a)**. Fast fourier transformations and Landau level fandiagrm plots as shown in **Fig. S9(b) – (g)** clarified 8 T (π Berry phase) and 21T (0.82π Berry phase) for $V_G = 0$V, 8 T (π Berry phase), 16.5 T (0 Berry phase) oscillations for $V_G = $ -120V , and 5 T (π Berry phase), 8 T(π Berry phase) and 28 T (0 Berry phase) for $V_G = $ -150V. Since the resistance maximum in V_G-R_{xx} indicated the existence of Dirac point around V_G = -120 – -130 V, the electric field effect changed the Fermi level of the bottom topological surface state whereas it gave less influence for the top topological surface state, demonstrating the nonequivalence Fermi level shift for the top and bottom topological surface by the electric field effect. In addition, we found additional trivial Fermi surface with oscillation frequencies ~16.5 and 28 T under the $V_G = $ -120 and -150 V and this is consistent with the previous report of the trivial surface accumulation layer induced by the electric field effect[7].
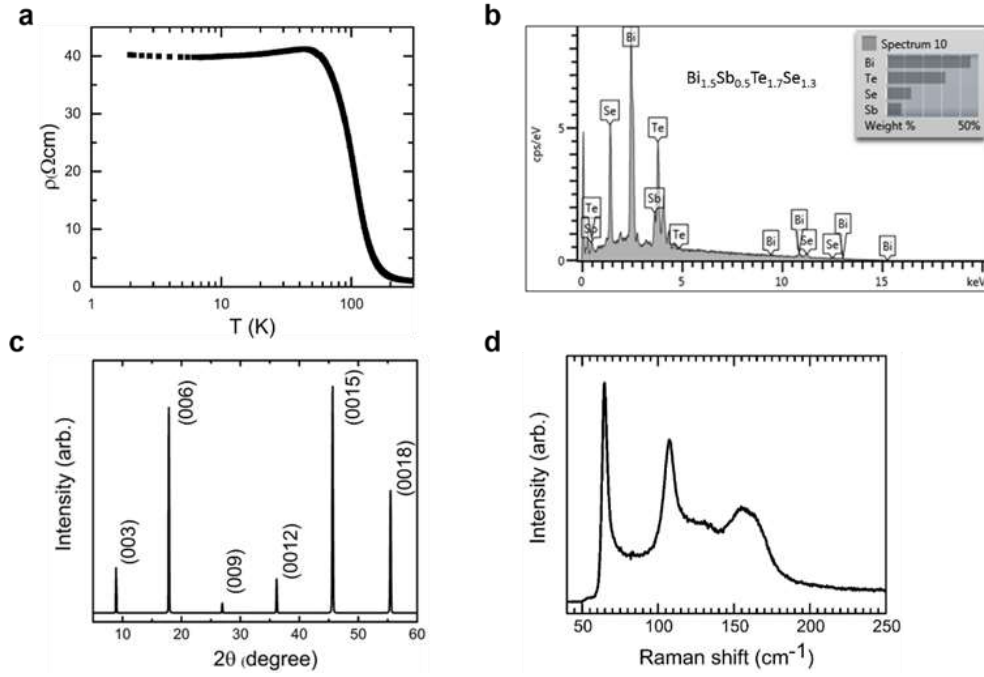
Figure S1. Characterization of BSTS single crystals. (a) Temperature dependence of electricl resistivity (ρ_{xx}). (b) EDX spectrum indicates the composition of bulk single crystal is $Bi_{1.5}Sb_{0.5}Te_{1.7}Se_{1.3}$. (c) Out of plane XRD pattern of bulk single crystal BSTS, all of diffraction peaks can be indexed as the (*00l*) (*l* = 3*n,* where n in integer). (d) Raman spectra of BSTS single crystal.
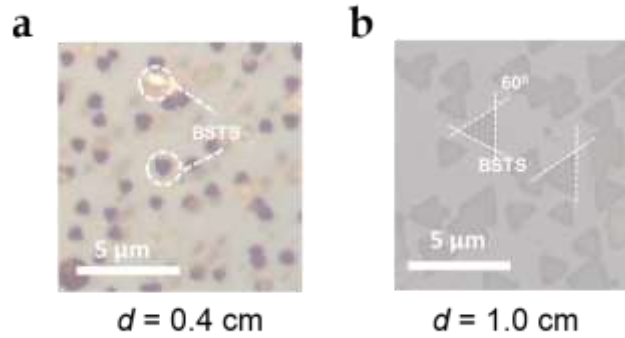

Figure S2. Influence of an inner tube diameter *d* on the nucleation process observed by the optical microscope. (a) *d* = 0.4 cm : small nuclei (< 1μm) with variable thicknesses from ultrathin (purple) to thick (yellow) (b) *d* = 1.0 cm : triangle or hexagonal NPs with almost same orientation and thickness. (Also see Fig. 2 (a) in the main text.)
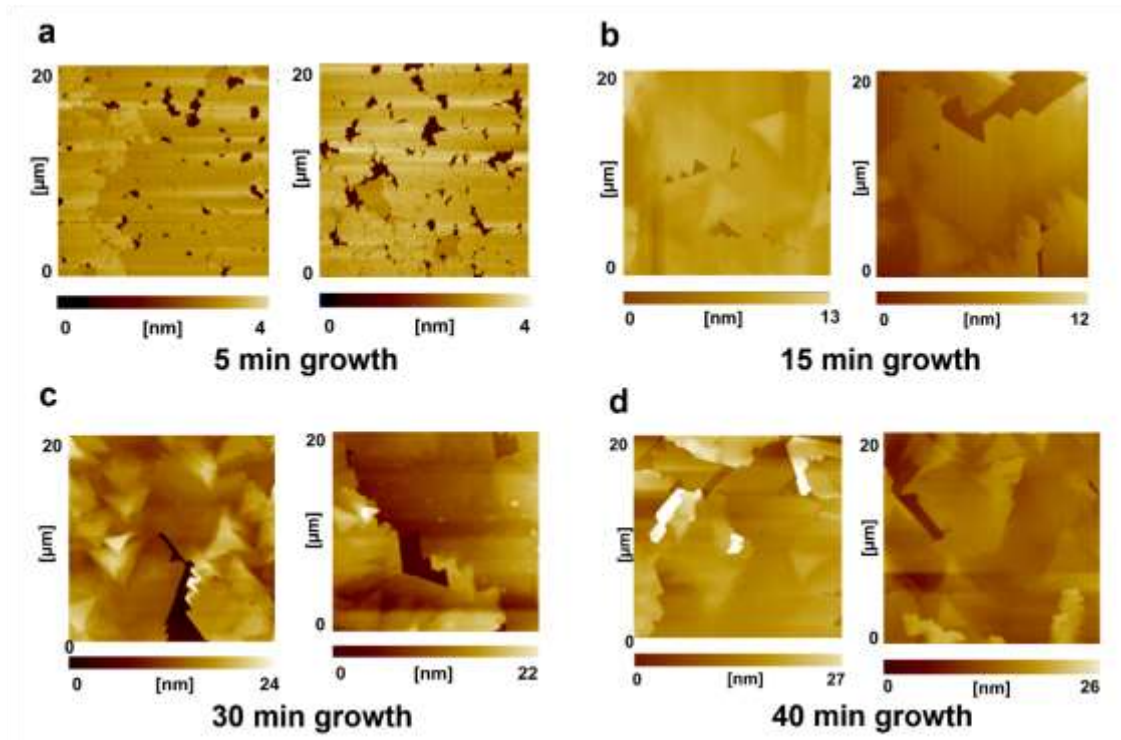
Figure S3. AFM image for the as - grown $Bi_{2-x}Sb_xTe_{3-y}Se_y$ thin film with an inner tube diameter d = 1.5 cm with different growh time (a) 5 min (b) 15 min (c) 30 min (d) 40 min.

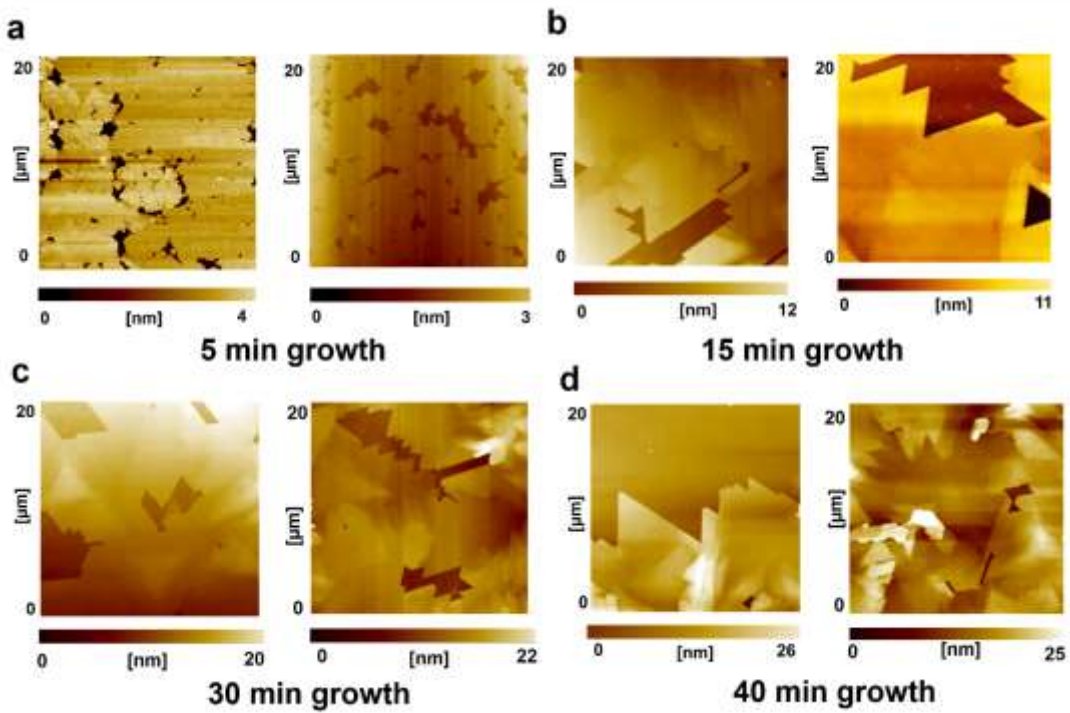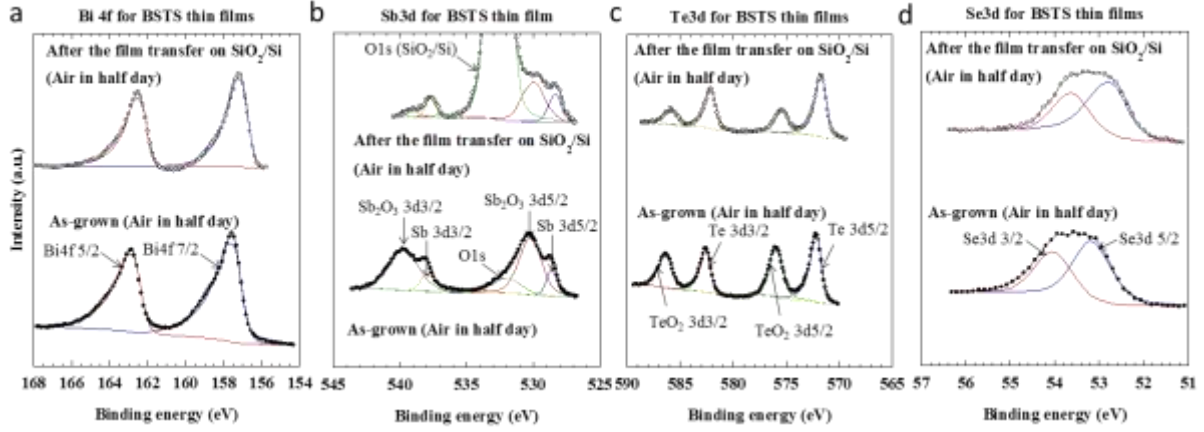**Figure S4.** AFM image for the transferred $Bi_{2-x}Sb_xTe_{3-y}Se_y$ thin film with an inner tube diameter d = 1.5 cm with different growh time (a) 5 min (b) 15 min (c) 30 min (d) 40 min.

Figure S5. XPS studies on $Bi_{2-x}Sb_xTe_{3-y}Se_y$ thin film with (a)Bi4f, (b)Sb3d, (c)Te3d, (d)Se3d. After the thin film growth, the as grown BSTS thin film ($1cm^2$) on the mica substrate was cutted in 4 mm^2 in the air for the film transfer process. After the film transfer process, both the as-grown film and the transferred film on the SiO_2/Si substrate were kept in the air for half day to clarify the additional oxidization originating from the film transfer process. XPS measurements were performed with the 45° angle between the a sample and a detecter. The incident beem was focused to a spot about 5 - 6 mm^2 region. Clear O1s peak after the film transfer is originated from the SiO_2/Si substrate. No obvious increase of TeO_2 and SbO_3 peak after the film transfer process indicated that the present film transfer process does not give any additional surface oxidization.
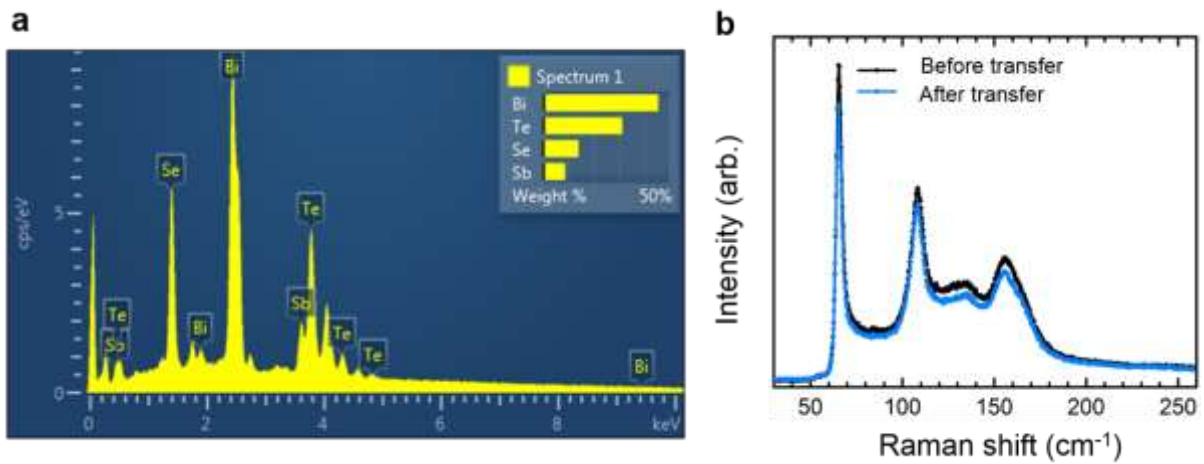

Figure S6. (a) EDX Spectra for a $Bi_{2-x}Sb_xTe_{3-y}Se_y$ thin film. (b) Raman Spectra for a $Bi_{2-x}Sb_xTe_{3-y}Se_y$ thin film before and after the film transfer process.

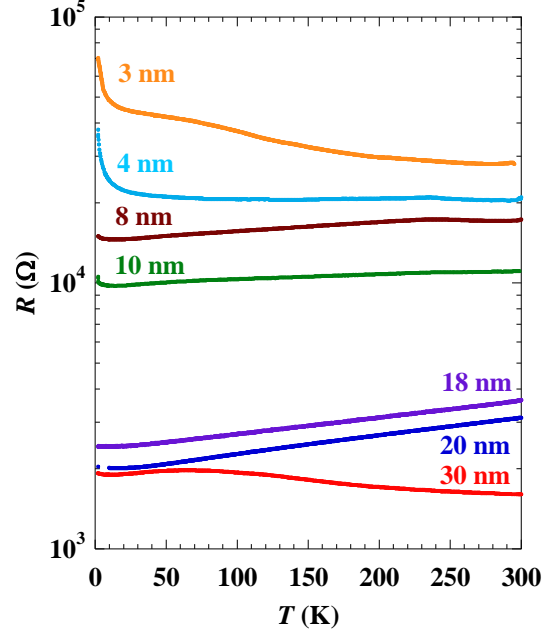**Figure S7**. Thickness dependence of the electrical resistance for the $Bi_{2-x}Sb_xTe_{3-y}Se_y$ ultrathin film from thicknesses from 3nm to 30 nm.

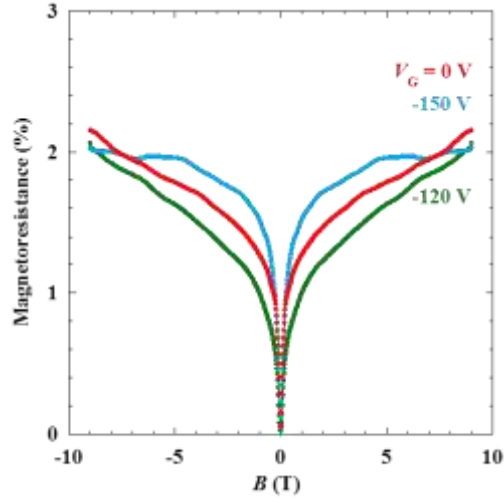**Figure S8**. Magnetic field (B) dependence of the magnetoressitance for a 18 nm $Bi_{2-x}Sb_xTe_{3-y}Se_y$ thin film with different back gate voltage (V_G) of 0, -120 and -150V.
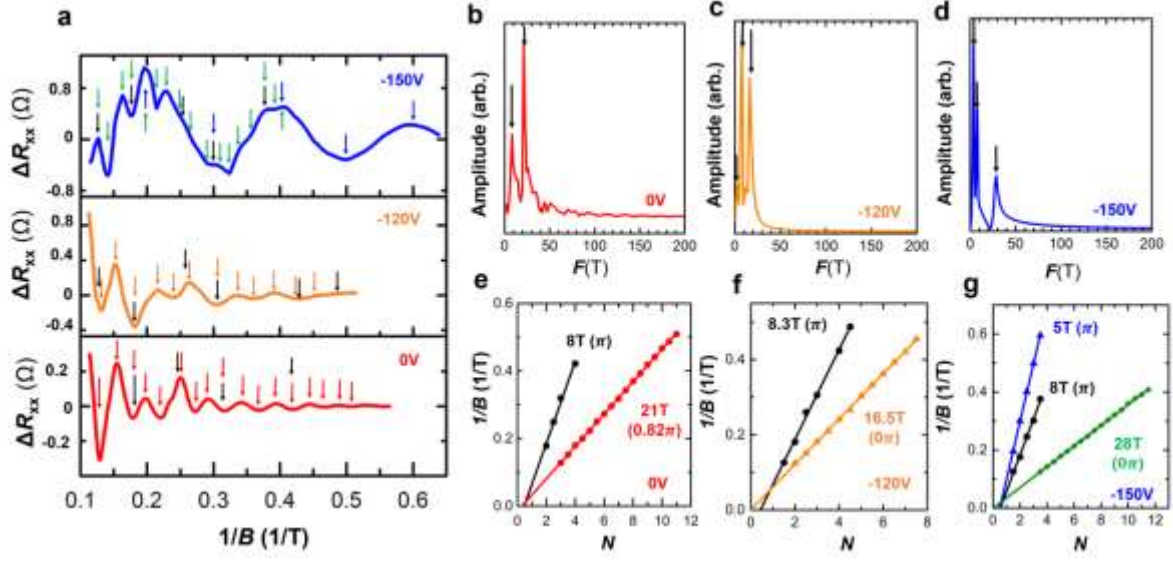
Figure S9. (a) Amplitude of the SdH oscillations as a function of $1/B$ with different back gate voltage (V_G) of 0, -120, and -150V. Arrows indicated peak and dip positions of oscillations extracting from fast Fourier transformation (FFT). (b – d) FFT of the oscillations for $V_G = 0$ V, -120 V, and -150 V. (e – g) Landau level (LL) fan diagram plot of ΔR_{xx}.

References

(1) Ren, Z.; Taskin, A. A.; Sasaki, S.; Segawa, K.; Ando, Y. *Phys. Rev. B* **2011**, 84, 165311.

(2) Tu, N. H.; Tanabe, Y.; Huynh, K. K.; Sato, Y.; Oguro, H.; Heguri, S.; Tsuda, K.; Terauchi, M.; Watanabe, K.; Tanigaki, K. *Appl. Phys. Lett.* **2014**, 105, 063104.

(3) Kong, D.; Cha, J. J.; Lai, K.; Peng, H.; Analytis, J. G.; Meister, S.; Chen, Y.; Zhang, H.-J.; Fisher, I. R.; Shen, Z.-X.; and Cui, Y. *ACS Nano*, **2011**, 5, 4698.

(4) Taskin, A. A.; Ren, Z.; Sasaki, S.; Segawa, K.; Ando, Y. *Phys .Rev. Lett.* **2011**, 107, 016801.

(5) Zhang, Y.; He, K.; Chang, C.-Z.; Song, C.-L.; Wang, L.-L.; Chen, X.; Jia, J.-F.; Fang, Z.; Dai, X.; Shan, W.-Y.; Shen, S.-Q.; Niu, Q.; Qi, X.-L.; Zhang, S.-C.; Ma, X.-C.; Xue, Q.-K. *Nat. Phys.* **2010**, 6, 584.

(6) Liao, J.; Ou, Y.; Feng, X.; Yang, S.; Lin, C.; Yang, W.; Wu, K.; He, K.; Ma, X.; Xue, Q. K.; Li, Y. *Phys. Rev. Lett.* **2015**, 114, 216601.

(7) Tu, N. H.; Tanabe, Y.; Satake, Y.; Huynh, K. K.; Tanigaki, K. *Nat. Commun.* **2016**, 7. 13763.